Check for updates

Geophysical Research Letters

RESEARCH LETTER
10.1029/2025GL118689

Orbitally-Driven Nutrient Pulses Linked to Early Cambrian Periodic Oxygenation and Animal Radiation

Yinggang Zhang[1,2], Benjamin J. W. Mills[2], Robert J. Newton[2], Tianchen He[3], Ailsa Roper[2], Tao Yang[4], and Maoyan Zhu[1,5]

[1]State Key Laboratory of Palaeobiology and Stratigraphy, Nanjing Institute of Geology and Palaeontology, Chinese Academy of Sciences, Nanjing, China, [2]School of Earth and Environment, University of Leeds, Leeds, UK, [3]College of Oceanography, Hohai University, Nanjing, China, [4]State Key Laboratory of Critical Earth Material Cycling and Mineral Deposits, School of Earth Sciences and Engineering, Nanjing University, Nanjing, China, [5]College of Earth and Planetary Sciences, University of Chinese Academy of Sciences, Beijing, China

Key Points:

- Carbon and sulfur isotope records from the early Cambrian show evidence of orbital cyclicity
- Biogeochemical modeling suggests that orbitally-driven nutrient pulses could drive long-period cyclic variations in the C-S-O cycles
- Low ocean sulfate levels were likely crucial in amplifying the C-S-O cycle responses to orbitally-driven nutrient pulses

Supporting Information:

Supporting Information may be found in the online version of this article.

Correspondence to:

M. Zhu and T. Yang,
myzhu@nigpas.ac.cn;
yangtao@nju.edu.cn

Citation:

Zhang, Y., Mills, B. J. W., Newton, R. J., He, T., Roper, A., Yang, T., & Zhu, M. (2025). Orbitally-driven nutrient pulses linked to early Cambrian periodic oxygenation and animal radiation. *Geophysical Research Letters*, *52*, e2025GL118689. https://doi.org/10.1029/2025GL118689

Received 5 AUG 2025
Accepted 15 OCT 2025

Author Contributions:

Conceptualization: Yinggang Zhang, Benjamin J. W. Mills, Tianchen He, Maoyan Zhu
Funding acquisition: Yinggang Zhang, Benjamin J. W. Mills, Tao Yang, Maoyan Zhu
Investigation: Yinggang Zhang
Methodology: Yinggang Zhang, Benjamin J. W. Mills, Ailsa Roper
Supervision: Benjamin J. W. Mills, Robert J. Newton, Tianchen He, Tao Yang, Maoyan Zhu
Validation: Yinggang Zhang, Benjamin J. W. Mills, Tianchen He
Visualization: Yinggang Zhang

© 2025. The Author(s).
This is an open access article under the terms of the Creative Commons Attribution License, which permits use, distribution and reproduction in any medium, provided the original work is properly cited.

Abstract During the Cambrian Explosion, episodic radiations of major animal phyla occurred in concert with repeated coupled carbon-sulfur isotope excursions. These isotope patterns are thought to reflect oscillations in atmospheric and shallow-marine O_2, which promoted animal diversification events. However, the driver for oxygenation pulses is unclear. Here we show that these synchronous carbon-sulfur isotope cycles and marine oxygenation pulses can be driven by long-period orbital forcing through effects on continental weathering and nutrient delivery. The impact of orbital forcing is explored using a combined climate-biogeochemical model. When forced with latitudinally-resolved insolation signals, the model produces long-term variations in nutrient weathering and carbon burial, which reproduces the co-variation of carbon-sulfur isotopes. We conclude that the oxygen-driven evolutionary changes in the early Cambrian can be explained by recurrent nutrient inputs to the ocean, resulting from climate change caused by long-period orbital cycles.

Plain Language Summary During the Cambrian Explosion, many major animal groups appeared in a relatively short period of time. These evolutionary bursts happened alongside seawater chemical changes which are thought to reflect variations in the amount of oxygen in Earth's oceans and atmosphere, which could set the pace of animal diversification. But the cause of these oxygen fluctuations has remained unclear. In this study, we show that slow changes in Earth's orbit may have played a key role. Our model shows that changing inputs of solar energy can change weathering processes on land and the flow of nutrients into the ocean, driving photosynthesis, and increased production of oxygen that occurs in pulses similar to those seen in animal evolution.

1. Introduction

During the early Cambrian, the rate of animal diversification accelerated, and most modern animal phyla appeared (Na & Kiessling, 2015), an event known as the Cambrian Explosion. This animal radiation occurred under a greenhouse climate condition, with atmospheric oxygen levels of perhaps 10%–50% of the present atmospheric level (PAL, where 1 PAL = 21% atm) (Mills et al., 2021; Sperling et al., 2013, 2015), and seawater sulfate concentrations of ~0.4–10 mM (Algeo et al., 2015). Increases in marine biodiversity appear to have followed an episodic pattern, where either reef-building archaeocyathan or the total animal species show biodiversity highs at ~2–3 million-year intervals. It coincided with repeated carbon and sulfur isotope excursions from ~524 to ~514 Ma (He et al., 2019) (million years ago; Figure 1). These isotope excursions are interpreted as reflecting periodic oscillation in atmospheric O_2 levels (He et al., 2019; G.-Y. Wei et al., 2018; G. Wei et al., 2021), implying parallel oscillation in shallow marine oxygen levels—a potential driver of biodiversity. Redox-sensitive geochemical proxies, including uranium and nitrogen isotopes (Wang et al., 2018), chromium isotope and cerium-anomaly data (W. Wei et al., 2018), support the occurrence of these oxygenation cycles; however, it is unknown what drove these periodic variations in Earth's seawater redox state.

Periodic changes at the Earth surface on the order of several million years (Myrs), such as biological turnover (Van Dam et al., 2006), carbon-cycle variations, and sea-level fluctuations (Boulila et al., 2018), have previously been linked to astronomical forcing through the long-period ~1.2 and ~2.4 Myr orbital cycles. Changes to these orbital parameters determine the distribution of solar radiation at the top of Earth's atmosphere and lead to climate fluctuations, which can subsequently promote changes in global biogeochemical cycles. Such orbital effects are

Writing – original draft:
Yinggang Zhang
Writing – review & editing:
Yinggang Zhang, Benjamin J. W. Mills, Robert J. Newton, Tianchen He, Ailsa Roper, Tao Yang, Maoyan Zhu

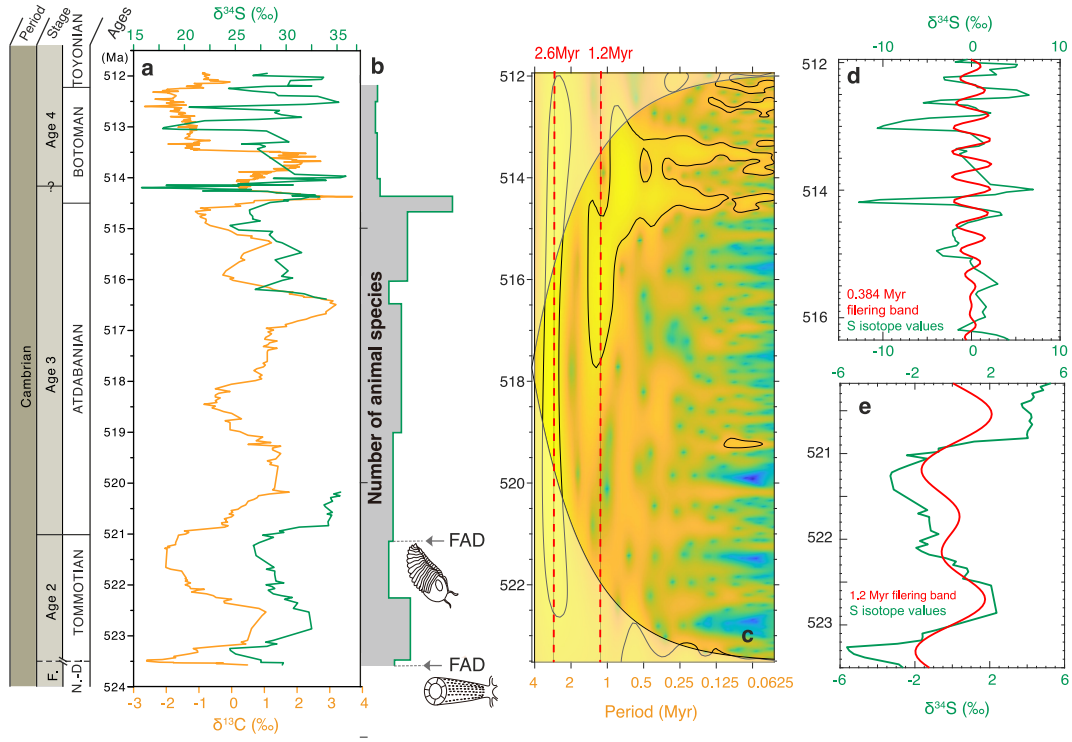

Figure 1. Carbonate carbon and carbonate-associated sulfate sulfur isotopes. (a) Records from Cambrian Stage 2 to Stage 4 from the southeastern Siberian Platform. (b) Number of animal species. (c) Wavelet analysis of the carbon isotope record, and (d–e) 384 Kyr and 1.2 Myr filter output from the sulfur isotope record.

well-documented on shorter timescales in the more recent geological past (most famously perhaps during Pleistocene glacial cycles (De Boer et al., 2014)), and the longer-term variations have been documented as far back as the Neoproterozoic and the early Phanerozoic (Sproson, 2020; T. Zhang et al., 2022).

Orbital variations can result in increased weathering rates and elevated nutrient fluxes into the ocean (Jenkyns, 2010), which can then drive the burial of organic carbon (Leloup & Paillard, 2023; Liu et al., 2024) and pyrite and thus oxygenate the Earth surface. In this paper, we propose that the long-period orbital forcing is responsible for the pulses of oxygenation and biological radiation observed during the Cambrian Explosion. To investigate this idea, we first conduct spectral analysis on published carbon-sulfur isotope records to determine whether these events are in phase with orbital cyclicity. We then use a climate-biogeochemical model to assess the effect of orbital variations on weathering, nutrient delivery, and global biogeochemistry.

2. Spectral Analysis and Climate-Biogeochemical Modeling

Following a standard spectral analysis procedure (Li et al., 2019; see Supporting Information S1), we analyzed the repeated carbon-sulfur isotope variations documented at the Siberian Platform (He et al., 2019) and a global carbon isotope compilation (Bowyer et al., 2022) (Figures S1–S7 in Supporting Information S1). Carbonate carbon isotope records spanning from 525 to 512 Ma show a prominent cyclicity with a frequency of around 2.6 Myr, along with more weakly expressed frequencies of ∼1.2 and ∼4.5 Myr (Figure 1 and Figures S1–S7 in Supporting Information S1). Meanwhile, the sulfur isotope record from Siberia shows a ∼385 Kyr cyclicity from ∼516.4 to ∼512 Ma, and ∼1.2 Myr cyclicity prior to ∼520 Ma (Figure 1). Regardless of detrending methods (Figure S1 in Supporting Information S1), the ∼2.6 Myr cyclicity in the carbon isotope records remains stable and exceeds a 95% false discovery rate-corrected confidence level (Hopkins et al., 2002) based on a smoothed window average red-noise fit (Weedon, 2022; Weedon et al., 2019) (Figures S2–S5 in Supporting Information S1). Alternative red-noise models (Figures S6–S7 in Supporting Information S1) also yield the ∼2.6 Myr cyclicity in the carbon isotope records. A ∼4 Myr data gap in the sulfur isotope record (Figure 1) prevents direct spectral detection of ∼2.6 Myr cycles, but correlations between the carbon and sulfur isotope data suggest that such a long-

19448007, 2025, 20, Downloaded from https://agupubs.onlinelibrary.wiley.com/doi/10.1029/2025GL118689 by NICE, National Institute for Health and Care Excellence, Wiley Online Library on [18/06/2026]. See the Terms and Conditions (https://onlinelibrary.wiley.com/terms-and-conditions) on Wiley Online Library for rules of use; OA articles are governed by the applicable Creative Commons License

19448007, 2025, 20, Downloaded from https://agupubs.onlinelibrary.wiley.com/doi/10.1029/2025GL118689 by NICE, National Institute for Health and Care Excellence, Wiley Online Library on [18/06/2026]. See the Terms and Conditions (https://onlinelibrary.wiley.com/terms-and-conditions) on Wiley Online Library for rules of use; OA articles are governed by the applicable Creative Commons License

term cyclicity (Figure S4 in Supporting Information S1) is also be present in the sulfur isotope record. We acknowledge that the relatively short length of the C-S isotope records (~12 Myr), and the time-uncertainty inherent in geological records of this age (Martinez & Dera, 2015), add challenges to the detection of long-period cyclicity. Nevertheless, ~3.45 Myr cycles have previously been identified in ~9 Myr sedimentary records (Wu et al., 2013), and ~4.5 Myr cycles in ~33 Myr successions (Sproson, 2020). Following these precedents, we applied Monte-Carlo age-random simulations (Figure S6–S7 in Supporting Information S1) to account for time uncertainties, and the ~2.6 Myr cyclicity in our data set remains sufficiently robust to warrant consideration of its potential drivers and biogeochemical impacts.

Our identified carbon isotope cyclicities (~1.2, ~2.6, and ~4.5 Myr) are consistent with those previously observed in the carbon cycle records for the early Phanerozoic (Sproson, 2020; Zhao et al., 2022). Similarly, the 385 Kyr and 1.2 Myr cyclicity detected in the sulfur isotope record align with those previously reported in Cambrian sediments (T. Zhang et al., 2022). This observed frequency combination corresponds to orbital cycles, demonstrating a likely coupling between the carbon-sulfur isotope variation and orbital cycles. Given that the observed isotopic and biodiversity variations are on similar timescales to orbital periodicity, we now explore whether the magnitude of the changes brought about by orbital variations could have resulted in the observed isotope excursions, and what degree of change in atmospheric oxygen levels might be expected. To solve this we use the SCION model (Mills et al., 2021, 2025), a long-term climate-biogeochemical model that uses a data structure of physical climate simulations (Donnadieu et al., 2006), to inform a 2D continental weathering scheme and a nondimensional ocean. The model provides continuous estimates for the chemical composition of the atmosphere and oceans and various geochemical proxies.

Because SCION uses a steady-state climate component without accounting for orbital variations, we incorporate orbital forcing by estimating the orbitally-induced temperature variation at each latitude band over time and superimposing these temperature deviations directly onto the model's 2D climate grids (Figure 2). In the absence of an astronomical model for the Cambrian period, and assuming that orbital parameters during this time were not fundamentally different from more recent intervals of deep time—though precise orbital phasing remain unresolved—we adopt the orbital solution spanning ~99 to ~89 Ma from previous work (Laskar et al., 2004). We acknowledge that solar luminosity during the early Cambrian was likely slightly lower than ~99–89 Ma, but this difference is expected to be minor and does not materially affect our interpretation of the orbital forcing patterns. The solution exhibits periodicities (~2.4 Myr, ~1.2 Myr, and ~405 Kyr) similar to the carbon-sulfur cyclicity observed in the early Cambrian records, and thus is used as an external orbital forcing in SCION.

To estimate the surface temperature deviations, we compare the insolation variations at a sample latitude of 65°N with the mean surface-air temperature variations of 40–80°N from foraminifer $\delta^{18}O$ data over the past 1,500–2,450 Kyr (De Boer et al., 2014) (Figure 2). The variations in solar insolation influence surface air temperature at the chosen latitude (Figure 2a). The conversion factor between solar insolation and air temperatures here is estimated at ~0.97°C/Wm^{-2} (Figure 2b). We use this value to impose orbitally-driven temperature variations in the SCION model (Figure 2c), and also explore its other potential effects on weathering and productivity. First, we explore potential temperature-driven changes in runoff using a previously calculated statistical relationship (Probst & Tardy, 1989), allowing us to impose 2D runoff variations in the model. Second, we note that simple ocean models like that within SCION have been shown to require ~5 times the P input to drive the same productivity rise as in more complex models (Longman et al., 2021), so to account for this we explore a potential five-fold wider range in temperature forcing from 0.97 to 5.82°C/Wm^{-2} (Figure S13 in Supporting Information S1). This wide range is also expected to account for uncertainties in this conversion factor and the partial influence of varying Earth surface system boundary conditions on the latitudinal temperature gradient, such as land-ocean distribution and orogeny (Scotese et al., 2021).

Finally, to better explore anoxia feedback, the SCION model is further modified to split the single ocean box into "shelf" and "interior ocean" zones (Wollast et al., 1993), and to update functions for redox-dependent phosphorus burial based on recent work (Alcott et al., 2019, 2022) (see supplemental materials). Except for these adjustments, the model structure and boundary conditions follow the original SCION model (Mills et al., 2021). Model uncertainty is estimated by running a 1,000-member ensemble in which key parameters are varied with ±20% uncertainty (Figure 3 and Figure S14 in Supporting Information S1).

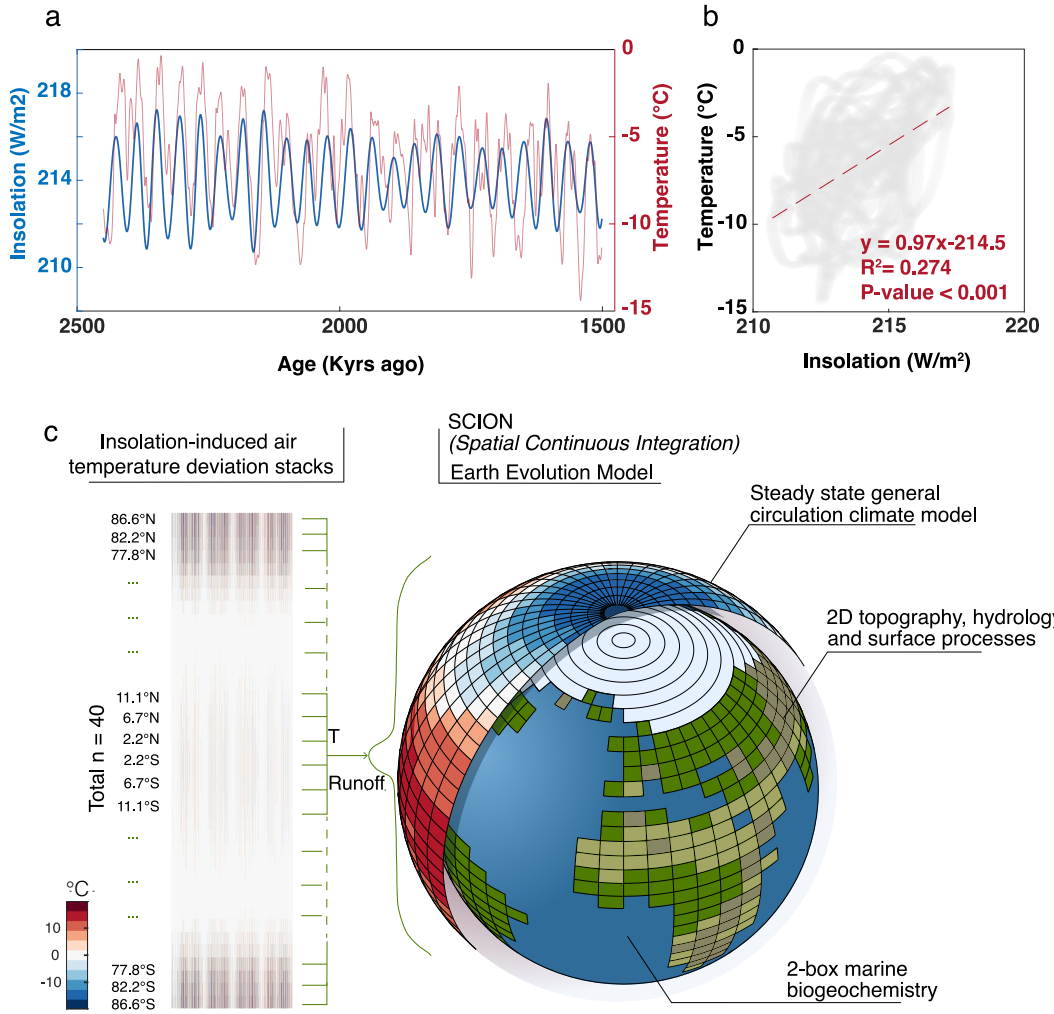

Figure 2. Solar forcing approximation in the SCION model. (a) Comparison of solar insolation at 65°N with air temperature variations over 40–80°N in the past 1,500–2,450 kyr. (b) A cross plot of solar insolation at 65°N with the air temperatures. (c) Insolation-induced air temperature 2D deviation stacks in the revised SCION model schematic diagram.

3. Results and Discussion

With the imposition of an artificial insolation forcing, we observe an oscillating pattern in the model output (Figure 3). The amplitudes of insolation vary most at high latitudes (Figure S8 in Supporting Information S1), which results in larger temperature fluctuations (Figure 2c) and therefore runoff fluctuations in these regions. The resulting global air temperature fluctuations are generally within 2°C (Figure S14 in Supporting Information S1). Temperature proxy records, such as $\delta^{18}O$ values, are often affected by diagenetic alteration and reliable records for early Cambrian are currently scarce (e.g., (Goldberg et al., 2021)), making it difficult to resolve such small fluctuations. This highlights the need for future high-resolution temperature proxy studies to further validate the magnitude of the temperature changes predicted here. With the large land area present at high latitudes during the Cambrian (Scotese, 2021) (Figure S9 in Supporting Information S1), weathering fluxes from high latitudes exert substantial control over the weathering signal (Figure S16 in Supporting Information S1). A large marine phosphate reservoir (Alcott et al., 2019) helps to dampen its responses to the high-frequency fluctuations in weathering supply (e.g., 400 kyr cycles). Consequently, while the weathering input of phosphorus tends to follow the insolation curve in Figure 2, the size of the marine phosphorus reservoir itself tends to increase where the amplitude of insolation variation is larger, and decrease when insolation variations are smaller (Figure 3a and Figure S14 in Supporting Information S1).

19448007, 2025, 20, Downloaded from https://agupubs.onlinelibrary.wiley.com/doi/10.1029/2025GL118689 by NICE, National Institute for Health and Care Excellence, Wiley Online Library on [18/06/2026]. See the Terms and Conditions (https://onlinelibrary.wiley.com/terms-and-conditions) on Wiley Online Library for rules of use; OA articles are governed by the applicable Creative Commons License

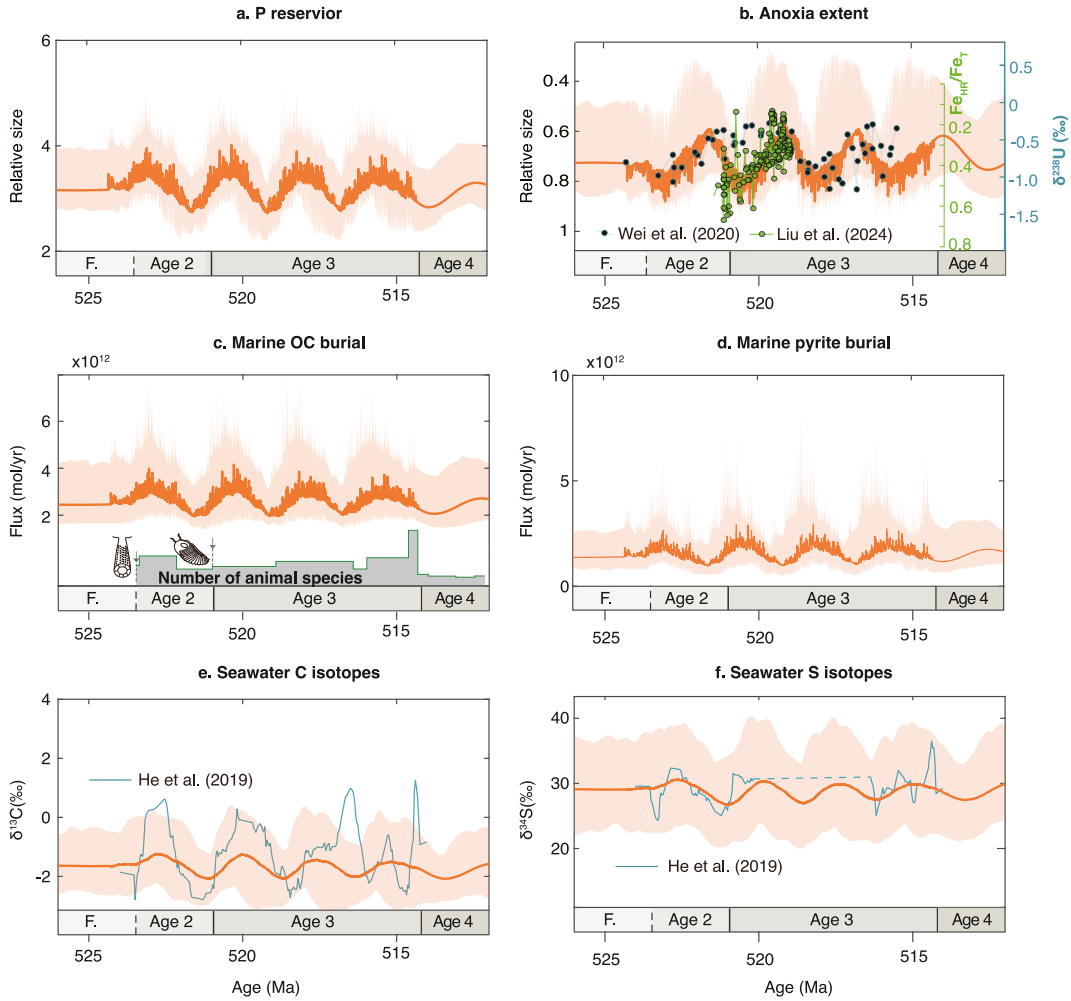

Figure 3. Model outputs with key parameters varied within 20% uncertainty. (a) Shelf nutrient phosphorus reservoir size. (b) Anoxic seafloor extent compared to uranium isotope and iron speciation data. (c–d) Marine organic carbon and pyrite burial on the shelf. (e–f) Carbon-sulfur isotopes. Full model outputs are shown in Figure S14 in Supporting Information S1.

This feature, alongside a large surface carbon reservoir in the Cambrian ocean (Mills et al., 2021), results in muted responses of the seawater carbon-sulfur isotopes to short-term (i.e., <100 kyr) weathering fluctuations (Leloup & Paillard, 2023). By contrast, long periods of increased phosphorus concentration (i.e., >1 Myr) drive widespread seafloor anoxia, increasing the burial rate of both organic carbon and pyrite (Figure 3). The modeled anoxia is largely consistent with redox proxy records, including uranium-isotope nadirs (G.-Y. Wei et al., 2020) and elevated reactive iron/total iron ratios from South China (Liu et al., 2024) across this interval (Figure 3b). Notably, marine anoxia predicted at the onset of Stage 3 is absent in the uranium-isotope record but manifest in the local iron-speciation record (Liu et al., 2024) and molybdenum isotope record (Dahl et al., 2019), highlighting the need for additional global redox proxy work to test this modeled scenario. Because organic carbon and pyrite burial are increasing and decreasing simultaneously, the model provides a qualitative fit to the carbon-sulfur isotopic couplings observed in the lower Cambrian successions as well as being consistent with other key boundary conditions (e.g., seawater sulfate concentration (Brennan et al., 2004) and atmospheric O_2 levels (Sperling et al., 2013, 2015), Figure S14 in Supporting Information S1). The rising limbs of the carbon-sulfur isotope curves—associated with higher nutrient inputs—are accompanied by increasing atmospheric (and therefore also shallow marine) O_2 levels. These generally coincide with Siberian biodiversity highs in the total animal species, including the first appearance of archaeocyaths (~524 Ma) and trilobites (~521 Ma). Conversely, the falling limbs—linked to reduced nutrient inputs and declining atmospheric O_2 levels—correspond to observed biodiversity declines (Figure 3c). Notably, modeled atmospheric O_2 maxima lag burial flux peaks by ~0.5 Myr

19448007, 2025, 20, Downloaded from https://agupubs.onlinelibrary.wiley.com/doi/10.1029/2025GL118689 by NICE, National Institute for Health and Care Excellence, Wiley Online Library on [18/06/2026]. See the Terms and Conditions (https://onlinelibrary.wiley.com/terms-and-conditions) on Wiley Online Library for rules of use; OA articles are governed by the applicable Creative Commons License

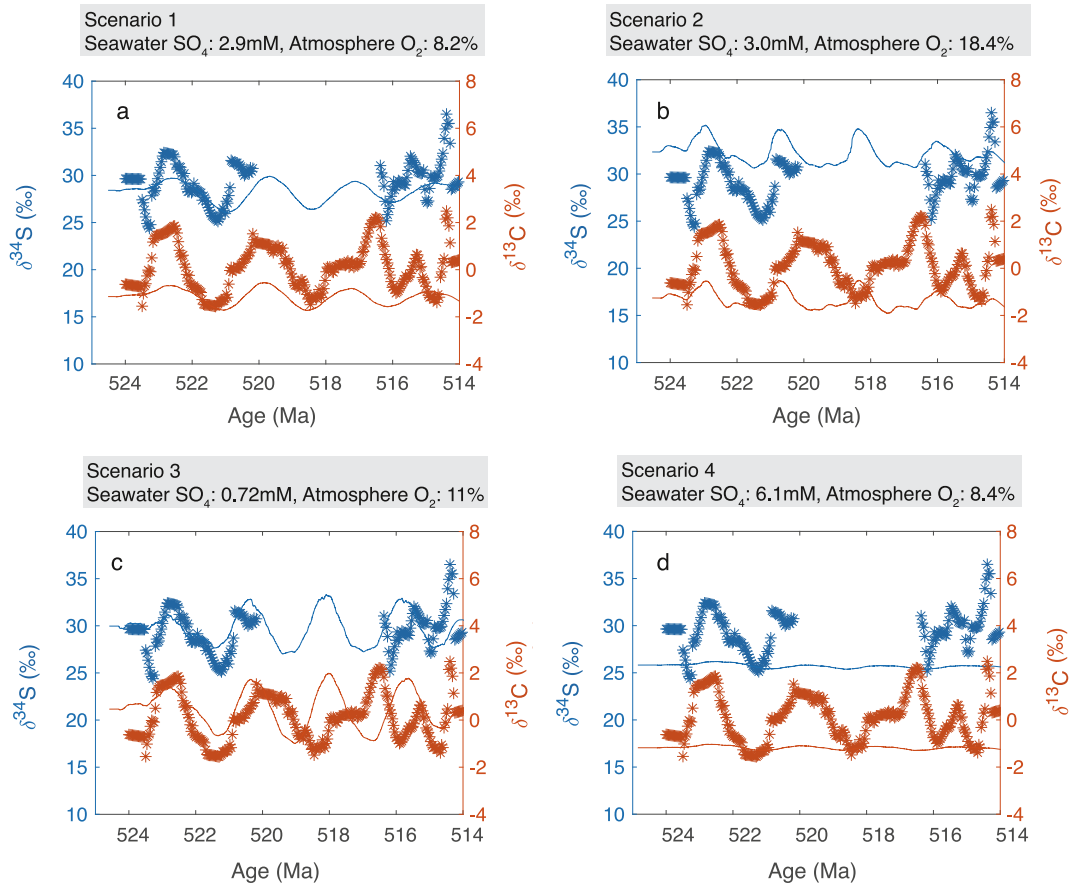

Figure 4. Isotope signal amplitudes for different sulfate and oxygen levels. The corresponding sulfate and oxygen levels in each scenario are shown at the top of each panel. (a) Scenario 1: low sulfate, low oxygen. (b) Scenario 2: low sufate, high oxygen. (c) Scenario 3: extremely low sufate, low oxygen. (d) Scenario 4: relatively high sulfate, low oxygen.

(Figure S12 in Supporting Information S1). This lag reflects the timescale of atmospheric O_2 responses to organic carbon and pyrite burial during the early Cambrian, but whether a similar delay is present in biodiversity responses remains uncertain due to the relatively low temporal resolution of available fossil data.

Here, the modeled $\delta^{13}C$-$\delta^{34}S$ variation range captures the detrended $\delta^{13}C$ and $\delta^{34}S$ record, but the modeled averages (shown by the dark orange line in Figures 3e and 3f) are more muted. It may be the case that more complex models with more explicit process representation would produce larger changes in phosphate inventories and larger isotopic swings under our mean calculated insolation-temperature relationship, as discussed earlier, and represented by the high end of our uncertainty range (Alcott et al., 2019; Longman et al., 2021). Alternatively, other biogeochemical factors could also amplify these isotopic signals, which we explore below.

The positively coupled carbon-sulfur isotope cycles that we observe in the geological record (and in our model) are a distinct feature of the Cambrian, whereas the long-term record in the Phanerozoic shows these isotope records to be negatively correlated (Garrels & Lerman, 1981). Usually, it is thought that high organic carbon burial would result in excess atmospheric O_2 production, which would limit rates of pyrite burial by limiting the prevalence of anaerobic environments (Garrels & Lerman, 1981). In Figure 4 we investigate the response of our modeled carbon-sulfur perturbations to different background seawater sulfate concentrations and atmospheric oxygen levels. These are achieved by modifying the sizes of initial reservoirs in the Earth surface and background phosphorus weathering inputs (see details in Supporting Information S1), and we choose our average insolation-temperature conversion factor of ~2.91°C/Wm^{-2}. Note that the many interlinked feedbacks in the model make the sulfate and oxygen concentrations to be co-dependent, meaning that the solutions for their background concentrations are not always integer values. Nevertheless, we can create model runs with low O_2 (~8%–11%

19448007, 2025, 20, Downloaded from https://agupubs.onlinelibrary.wiley.com/doi/10.1029/2025GL118689 by NICE, National Institute for Health and Care Excellence, Wiley Online Library on [18/06/2026]. See the Terms and Conditions (https://onlinelibrary.wiley.com/terms-and-conditions) on Wiley Online Library for rules of use; OA articles are governed by the applicable Creative Commons License

19448007, 2025, 20, Downloaded from https://agupubs.onlinelibrary.wiley.com/doi/10.1029/2025GL118689 by NICE, National Institute for Health and Care Excellence, Wiley Online Library on [18/06/2026]. See the Terms and Conditions (https://onlinelibrary.wiley.com/terms-and-conditions) on Wiley Online Library for rules of use; OA articles are governed by the applicable Creative Commons License

atm) and either very low (0.72 mM), low (2.9 mM) or moderate (6.1 mM) sulfate concentrations, and an additional high oxygen run (18.4% atm) to test how these affect the isotope cycles.

In the low oxygen—low sulfate (2.9 mM) scenario (Figure 4a), the modeled variations of seawater carbon and sulfur isotopes are positively correlated and in pace with the insolation modulation cycles (~2.4 Myr) and the sulfur isotopes show similar amplitude changes relative to the geological record, while those of carbon are more muted ($\Delta\delta^{13}C > 1‰$ and $\Delta\delta^{34}S > 4‰$). With a similar sulfate concentration but under high atmospheric oxygen concentration (Figure 4b), we see a slight reduction in the amplitudes of $\delta^{13}C$ and $\delta^{34}S$ (~1‰ for $\delta^{13}C$ and ~4‰ for $\delta^{34}S$) and a reduced duration of the positive excursions, which may be expected with less prevalence of anoxia and therefore less phosphorus recycling. If we instead maintain atmospheric O_2 at low concentrations and decrease marine sulfate levels to be close to the lower limits proposed for the early Cambrian (~0.7 mM (He et al., 2019)), the amplitudes of C-S isotopic fluctuations are increased ($\Delta\delta^{13}C > 2‰$ and $\Delta\delta^{34}S > 5‰$; Figure 4c). In contrast, if we increase the sulfate level, the carbon-sulfur isotopic fluctuations are almost completely flattened (Figure 4d).

Our analysis in Figure 4 suggests that large-scale co-variation in organic carbon and pyrite burial rates (and thus, pulsed oxygenation of the atmosphere and surface ocean) is a feature of a low oceanic sulfate system and is less dependent on atmospheric oxygen levels. When ocean sulfate levels are extremely low, an orbitally-paced weathering influx of sulfate from the continents—applied by the presence of large high-latitude land masses during the Cambrian (Scotese, 2021) (Figure S16 in Supporting Information S1)—can change the marine sulfate concentration substantially and would lead to large variations in the pyrite burial rate (Figure S17 in Supporting Information S1). This highly variable rate of pyrite burial impacts the $\delta^{34}S$ record directly (as pyrite is isotopically lighter than sulfate), but it also makes atmospheric and oceanic oxygen levels more variable, which then impacts the carbon cycle. As a result, the superimposed variations of organic carbon and pyrite burial during low-sulfate conditions should result in large amplitude cycles in seawater $\delta^{13}C$ and $\delta^{34}S$ records.

Another key time of low sulfate concentrations was the Early Jurassic (Newton et al., 2011), which had a high atmospheric oxygen level (Mills et al., 2021). During that time, the $\delta^{13}C$ record is paced by orbital modulation cycles (~2.5 Myr) and has a magnitude of around 1‰–2‰ (Storm et al., 2020), similar to the magnitude of the early Cambrian $\delta^{13}C$ cycles (~2%–3%). As shown in our model (Figure 4b), this example suggests that the higher Jurassic level of atmospheric oxygen did not greatly affect the Earth-system response to cyclical weathering inputs induced by orbital variations. Our hypothesis, that high seawater sulfate concentration reduces both carbon and sulfur cycle variability, is consistent with the observation that the general coupling of the carbon-sulfur isotope records becomes weaker after the mid-to-late Paleozoic (Gill et al., 2007) when long-term sulfate levels appear to have risen (Algeo et al., 2015). These findings also suggest that mid-Proterozoic isotope records might exhibit a similar cyclicity, given the generally low sulfate levels expected at this time. Currently, sufficiently high resolution isotope records are not available to test this.

Overall, long-period effects of astronomical forcing provide a possible explanation for the ~2.6 Myr cyclicity observed in carbon-sulfur isotope records during the Cambrian Explosion. This mechanism can account for the timing of surface ocean oxygenation pulses and associated episodes of ecological expansion. Interestingly, shorter-period effects appear to have been buffered by the large nutrient and inorganic carbon reservoirs in the Cambrian ocean. Key to these environmental upheavals was concentrated land distributions at high latitudes during early Cambrian and an early Cambrian ocean with low sulfate concentrations, which was very sensitive to varying sulfate inputs from the continents. It also highlights the important role of low-sulfate conditions in increasing Earth system sensitivity to external forcings. Such a low sulfate ocean appears to have allowed for significant changes in the burial rates of organic carbon and pyrite, periodic oxygenation of the atmosphere and surface ocean, and ultimately, the boom and bust of Cambrian radiation.

4. Conclusion

Our modeling results suggest that astronomical forcing played a critical role in driving cyclical climate and biogeochemical dynamics during the early Cambrian. In the model, these oscillations were most pronounced at high latitudes, where larger land areas and stronger insolation variability controlled continental weathering and phosphorus weathering fluxes. Under conditions of low marine sulfate and with a large land area present at high latitudes, as inferred for the early Cambrian, the weathering inputs of phosphorus significantly modulated the

19448007, 2025, 20, Downloaded from https://agupubs.onlinelibrary.wiley.com/doi/10.1029/2025GL118689 by NICE, National Institute for Health and Care Excellence, Wiley Online Library on [18/06/2026]. See the Terms and Conditions (https://onlinelibrary.wiley.com/terms-and-conditions) on Wiley Online Library for rules of use; OA articles are governed by the applicable Creative Commons License

burial of organic carbon and pyrite, leading to positively correlated $\delta^{13}C$ and $\delta^{34}S$ isotope values that broadly match the pacing of those observed in the geological record.

This study highlights the importance of low oceanic sulfate concentrations in enhancing Earth system sensitivity to external orbital forcings. When sulfate availability is limited, orbitally-driven phosphorus weathering inputs can produce substantial shifts in pyrite burial and oxygen levels, thereby amplifying isotopic signals and shaping the timing and intensity of redox fluctuations. These conditions likely contributed to the pulsed nature of the Cambrian radiation pattern. Thus, long-period astronomical forcing, modulated by sulfate-dependent feedbacks, offers a new framework for understanding both the isotope record and the episodic nature of early animal diversification during the early Cambrian. Such long-period cyclicity may also be applied to other geological periods that saw biogeochemical oscillations and oceanic redox on these timescales.

Conflict of Interest

The authors declare no conflicts of interest relevant to this study.

Data Availability Statement

The C and S isotope data plotted in Figures 1 and 3 are documented in (He et al., 2019), while air temperature data plotted in Figure 2a are from (De Boer et al., 2014). The modeling results in Figures 3 and 4 can be obtained using the revised SCION model, which can be found in (Y. Zhang et al., 2025). The U isotope data in Figure 3 are from (G.-Y. Wei et al., 2020), and its data starting age anchor is updated from (G. Wei et al., 2021). The Iron speciation data across in Figure 3 are from (Liu et al., 2024).

Acknowledgments

This work was supported by the National Key Research and Development Program of China (2022YFF0800100), the National Natural Science Foundation of China (41888101 and 42402312), and the Natural Environment Research Council (NE/N018559/1 to RJN, NE/S009663/1 to BJWM). YZ also acknowledges support from the Jiangsu Funding Program for Excellent Postdoctoral Talent. We thank Dr Mathieu Martinez for his generous sharing of Monte Carlo Markov chain Bchron simulation scripts. We also appreciate Dr Sarah Feakins's editorial guidance and the constructive comments from Chenyi Tu and one anonymous reviewer, which greatly improved the manuscript.

References

Alcott, L. J., Mills, B. J. W., Bekker, A., & Poulton, S. W. (2022). Earth's great oxidation event facilitated by the rise of sedimentary phosphorus recycling. *Nature Geoscience*, *15*(3), 210–215. https://doi.org/10.1038/s41561-022-00906-5

Alcott, L. J., Mills, B. J. W., & Poulton, S. W. (2019). Stepwise earth oxygenation is an inherent property of global biogeochemical cycling. *Science*, *366*(6741), 1333–1337. https://doi.org/10.1126/science.aax6459

Algeo, T. J., Luo, G. M., Song, H. Y., Lyons, T. W., & Canfield, D. E. (2015). Reconstruction of secular variation in seawater sulfate concentrations. *Biogeosciences*, *12*(7), 2131–2151. https://doi.org/10.5194/bg-12-2131-2015

Boulila, S., Laskar, J., Haq, B. U., Galbrun, B., & Hara, N. (2018). Long-term cyclicities in Phanerozoic sea-level sedimentary record and their potential drivers. *Global and Planetary Change*, *165*(August 2017), 128–136. https://doi.org/10.1016/j.gloplacha.2018.03.004

Bowyer, F. T., Zhuravlev, A. Y., Wood, R., Shields, G. A., Zhou, Y., Curtis, A., et al. (2022). Calibrating the temporal and spatial dynamics of the ediacaran—Cambrian radiation of animals. *Earth-Science Reviews*, *225*, 103913. https://doi.org/10.1016/j.earscirev.2021.103913

Brennan, S. T., Lowenstein, T. K., & Horita, J. (2004). Seawater chemistry and the advent of biocalcification. *Geology*, *32*(6), 473–476. https://doi.org/10.1130/G20251.1

Dahl, T. W., Connelly, J. N., Li, D., Kouchinsky, A., Gill, B. C., Porter, S., et al. (2019). Atmosphere–ocean oxygen and productivity dynamics during early animal radiations. *Proceedings of the National Academy of Sciences*, *116*(39), 19352–19361. https://doi.org/10.1073/pnas.1901178116

De Boer, B., Lourens, L. J., & Van De Wal, R. S. W. (2014). Persistent 400,000-year variability of Antarctic ice volume and the carbon cycle is revealed throughout the Plio-Pleistocene. *Nature Communications*, *5*(1), 2999. https://doi.org/10.1038/ncomms3999

Donnadieu, Y., Goddéris, Y., Pierrehumbert, R., Dromart, G., Jacob, R., & Fluteau, F. (2006). A GEOCLIM simulation of climatic and biogeochemical consequences of Pangea breakup. *Geochemistry, Geophysics, Geosystems*, *7*(11), Q11019. https://doi.org/10.1029/2006GC001278

Garrels, R. M., & Lerman, A. (1981). Phanerozoic cycles of sedimentary carbon and sulfur. *Proceedings of the National Academy of Sciences*, *78*(8), 4652–4656. https://doi.org/10.1073/pnas.78.8.4652

Gill, B. C., Lyons, T. W., & Saltzman, M. R. (2007). Parallel, high-resolution carbon and sulfur isotope records of the evolving Paleozoic marine sulfur reservoir. *Palaeogeography, Palaeoclimatology, Palaeoecology*, *256*(3–4), 156–173. https://doi.org/10.1016/j.palaeo.2007.02.030

Goldberg, S. L., Present, T. M., Finnegan, S., & Bergmann, K. D. (2021). A high-resolution record of early paleozoic climate. *Proceedings of the National Academy of Sciences*, *118*(6), e2013083118. https://doi.org/10.1073/pnas.2013083118

He, T., Zhu, M., Mills, B. J. W., Wynn, P. M., Zhuravlev, A. Y., Tostevin, R., et al. (2019). Possible links between extreme oxygen perturbations and the Cambrian radiation of animals. *Nature Geoscience*, *12*(6), 468–474. https://doi.org/10.1038/s41561-019-0357-z

Hopkins, A. M., Miller, C. J., Connolly, A. J., Genovese, C., Nichol, R. C., & Wasserman, L. (2002). A new source detection algorithm using the false-discovery rate. *Astronomical Journal*, *123*(2), 1086–1094. https://doi.org/10.1086/338316

Jenkyns, H. C. (2010). Geochemistry of oceanic anoxic events. *Geochemistry, Geophysics, Geosystems*, *11*(3), Q03004. https://doi.org/10.1029/2009GC002788

Laskar, J., Robutel, P., Joutel, F., Gastineau, M., Correia, A. C. M., & Levrard, B. (2004). A long-term numerical solution for the insolation quantities of the Earth. *Astronomy and Astrophysics*, *428*(1), 261–285. https://doi.org/10.1051/0004-6361:20041335

Leloup, G., & Paillard, D. (2023). Multi-million-year cycles in modelled $\delta^{13}C$ as a response to astronomical forcing of organic matter fluxes. *Earth System Dynamics*, *14*(2), 291–307. https://doi.org/10.5194/esd-14-291-2023

Li, M., Hinnov, L., & Kump, L. (2019). Acycle: Time-series analysis software for paleoclimate research and education. *Computers & Geosciences*, *127*(February), 12–22. https://doi.org/10.1016/j.cageo.2019.02.011

Liu, Y., Bowyer, F. T., Zhu, M., Xiong, Y., He, T., Han, M., et al. (2024). Marine redox and nutrient dynamics linked to the Cambrian radiation of animals. *Geology*, *52*(9), 729–734. https://doi.org/10.1130/G52220.1

Longman, J., Mills, B. J. W., Manners, H. R., Gernon, T. M., & Palmer, M. R. (2021). Late Ordovician climate change and extinctions driven by elevated volcanic nutrient supply. *Nature Geoscience*, *14*(12), 924–929. https://doi.org/10.1038/s41561-021-00855-5

Martinez, M., & Dera, G. (2015). Orbital pacing of carbon fluxes by a ∼9-my eccentricity cycle during the mesozoic. *Proceedings of the National Academy of Sciences*, *112*(41), 12604–12609. https://doi.org/10.1073/pnas.1419946112

Mills, B. J. W., Donnadieu, Y., & Goddéris, Y. (2021). Spatial continuous integration of Phanerozoic global biogeochemistry and climate. *Gondwana Research*, *100*, 73–86. https://doi.org/10.1016/j.gr.2021.02.011

Mills, B. J. W., Le Hir, G., Merdith, A., Gurung, K., Bowyer, F. T., Krause, A. J., et al. (2025). Exploring Neoproterozoic climate and biogeochemical evolution in the SCION model. *Global and Planetary Change*, *249*, 104791. https://doi.org/10.1016/j.gloplacha.2025.104791

Na, L., & Kiessling, W. (2015). Diversity partitioning during the Cambrian radiation. *Proceedings of the National Academy of Sciences of the United States of America*, *112*(15), 4702–4706. https://doi.org/10.1073/pnas.1424985112

Newton, R. J., Reeves, E. P., Kafousia, N., Wignall, P. B., Bottrell, S. H., & Sha, J. G. (2011). Low marine sulfate concentrations and the isolation of the European epicontinental sea during the early Jurassic. *Geology*, *39*(1), 7–10. https://doi.org/10.1130/G31326.1

Probst, J.-L., & Tardy, Y. (1989). Global runoff fluctuations during the last 80 years in relation to world temperature change. *American Journal of Science*, *289*(3), 267–285. https://doi.org/10.2475/ajs.289.3.267

Scotese, C. R. (2021). An atlas of phanerozoic paleogeographic maps: The seas come in and the seas go out. *Annual Review of Earth and Planetary Sciences*, *49*(1), 679–728. https://doi.org/10.1146/annurev-earth-081320-064052

Scotese, C. R., Song, H., Mills, B. J. W., & van der Meer, D. G. (2021). Phanerozoic paleotemperatures: The Earth's changing climate during the last 540 million years. *Earth-Science Reviews*, *215*, 103503. https://doi.org/10.1016/j.earscirev.2021.103503

Sperling, E. A., Frieder, C. A., Raman, A. V., Girguis, P. R., Levin, L. A., & Knoll, A. H. (2013). Oxygen, ecology, and the Cambrian radiation of animals. *Proceedings of the National Academy of Sciences of the United States of America*, *110*(33), 13446–13451. https://doi.org/10.1073/pnas.1312778110

Sperling, E. A., Wolock, C. J., Morgan, A. S., Gill, B. C., Kunzmann, M., Halverson, G. P., et al. (2015). Statistical analysis of iron geochemical data suggests limited late proterozoic oxygenation. *Nature*, *523*(7561), 451–454. https://doi.org/10.1038/nature14589

Sproson, A. D. (2020). Pacing of the latest ordovician and silurian carbon cycle by a ∼4.5 myr orbital cycle. *Palaeogeography, Palaeoclimatology, Palaeoecology*, *540*, 109543. https://doi.org/10.1016/j.palaeo.2019.109543

Storm, M. S., Hesselbo, S. P., Jenkyns, H. C., Ruhl, M., Ullmann, C. V., Xu, W., et al. (2020). Orbital pacing and secular evolution of the Early Jurassic carbon cycle. *Proceedings of the National Academy of Sciences of the United States of America*, *117*(8), 3974–3982. https://doi.org/10.1073/pnas.1912094117

Van Dam, J. A., Abdul Aziz, H., Sierra, M. Á. Á., Hilgen, F. J., Van Den Hoek Ostende, L. W., Lourens, L. J., et al. (2006). Long-period astronomical forcing of mammal turnover. *Nature*, *443*(7112), 687–691. https://doi.org/10.1038/nature05163

Wang, D., Ling, H. F., Struck, U., Zhu, X. K., Zhu, M., He, T., et al. (2018). Coupling of ocean redox and animal evolution during the Ediacaran-Cambrian transition. *Nature Communications*, *9*(1), 1–8. https://doi.org/10.1038/s41467-018-04980-5

Weedon, G. P. (2022). Problems with the current practice of spectral analysis in cyclostratigraphy: Avoiding false detection of regular cyclicity. *Earth-Science Reviews*, *235*, 104261. https://doi.org/10.1016/j.earscirev.2022.104261

Weedon, G. P., Page, K. N., & Jenkyns, H. C. (2019). Cyclostratigraphy, stratigraphic gaps and the duration of the Hettangian stage (Jurassic): Insights from the Blue Lias formation of southern Britain. *Geological Magazine*, *156*(9), 1469–1509. https://doi.org/10.1017/S0016756818000808

Wei, G., Planavsky, N. J., He, T., Zhang, F., Stockey, R. G., Cole, D. B., et al. (2021). Global marine redox evolution from the late Neoproterozoic to the early Paleozoic constrained by the integration of Mo and U isotope records. *Earth-Science Reviews*, *214*(January), 103506. https://doi.org/10.1016/j.earscirev.2021.103506

Wei, G.-Y., Planavsky, N. J., Tarhan, L. G., Chen, X., Wei, W., Li, D., & Ling, H.-F. (2018). Marine redox fluctuation as a potential trigger for the Cambrian explosion. *Geology*, *46*(7), 587–590. https://doi.org/10.1130/G40150.1

Wei, G.-Y., Planavsky, N. J., Tarhan, L. G., He, T., Wang, D., Shields, G. A., et al. (2020). Highly dynamic marine redox state through the Cambrian explosion highlighted by authigenic $\delta^{238}U$ records. *Earth and Planetary Science Letters*, *544*, 116361. https://doi.org/10.1016/j.epsl.2020.116361

Wei, W., Frei, R., Gilleaudeau, G. J., Li, D., Wei, G.-Y., Chen, X., & Ling, H.-F. (2018). Oxygenation variations in the atmosphere and shallow seawaters of the Yangtze platform during the Ediacaran period: Clues from Cr-isotope and Ce-anomaly in carbonates. *Precambrian Research*, *313*, 78–90. https://doi.org/10.1016/j.precamres.2018.05.009

Wollast, R., Mackenzie, F. T., & Chou, L. (1993). Interactions of C, N, P and S biogeochemical cycles and global change. *Global Environmental Change*. https://doi.org/10.1007/978-3-642-76064-8

Wu, H., Zhang, S., Hinnov, L. A., Jiang, G., Feng, Q., Li, H., & Yang, T. (2013). Time-calibrated Milankovitch cycles for the late Permian. *Nature Communications*, *4*(1), 2452. https://doi.org/10.1038/ncomms3452

Zhang, T., Li, Y., Fan, T., Da Silva, A.-C., Shi, J., Gao, Q., et al. (2022). Orbitally-paced climate change in the early Cambrian and its implications for the history of the solar system. *Earth and Planetary Science Letters*, *583*, 117420. https://doi.org/10.1016/j.epsl.2022.117420

Zhang, Y., Mills, B., & Roper, A. (2025). Orbitally-driven nutrient pulses linked to early Cambrian periodic oxygenation and animal radiation (SCION double_box ocean codes) (v 1.1.6) [Software]. *Zenodo*. https://doi.org/10.5281/zenodo.17241225

Zhao, Z., Thibault, N. R., Dahl, T. W., Schovsbo, N. H., Sørensen, A. L., Rasmussen, C. M. Ø., & Nielsen, A. T. (2022). Synchronizing rock clocks in the late Cambrian. *Nature Communications*, *13*(1), 1990. https://doi.org/10.1038/s41467-022-29651-4

References From the Supporting Information

Berner, R. A. (2006). GEOCARBSULF: A combined model for Phanerozoic atmospheric O_2 and CO_2. *Geochimica et Cosmochimica Acta*, *70*(23 SPEC. ISS.), 5653–5664. https://doi.org/10.1016/j.gca.2005.11.032

Huybers, P. (2006). Early Pleistocene glacial cycles and the integrated summer insolation forcing. *Science*, *313*(5786), 508–511. https://doi.org/10.1126/science.1125249

Kocken, I. J., Cramwinckel, M. J., Zeebe, R. E., Middelburg, J. J., & Sluijs, A. (2019). The 405 kyr and 2.4 myr eccentricity components in Cenozoic carbon isotope records. *Climate of the Past*, *15*(1), 91–104. https://doi.org/10.5194/cp-15-91-2019

Lenton, T. M., Daines, S. J., & Mills, B. J. W. (2018). COPSE reloaded: An improved model of biogeochemical cycling over Phanerozoic time. *Earth-Science Reviews*, *178*, 1–28. https://doi.org/10.1016/j.earscirev.2017.12.004

Lourens, L. J. (2021). The variation of the Earth's movements (orbital, tilt, and precession) and climate change. In *Climate change*. Elsevier B.V. https://doi.org/10.1016/b978-0-12-821575-3.00028-1

19448007, 2025, 20, Downloaded from https://agupubs.onlinelibrary.wiley.com/doi/10.1029/2025GL118689 by NICE, National Institute for Health and Care Excellence, Wiley Online Library on [18/06/2026]. See the Terms and Conditions (https://onlinelibrary.wiley.com/terms-and-conditions) on Wiley Online Library for rules of use; OA articles are governed by the applicable Creative Commons License

Maffre, P., Ladant, J.-B., Moquet, J.-S., Carretier, S., Labat, D., & Goddéris, Y. (2018). Mountain ranges, climate and weathering. Do orogens strengthen or weaken the silicate weathering carbon sink? *Earth and Planetary Science Letters*, *493*, 174–185. https://doi.org/10.1016/j.epsl.2018.04.034

Meyers, S. R. (2012). Seeing red in cyclic stratigraphy: Spectral noise estimation for astrochronology. *Paleoceanography*, *27*(3), PA3328. https://doi.org/10.1029/2012PA002307

Mills, B. J. W., Krause, A. J., Jarvis, I., & Cramer, B. D. (2023). Evolution of atmospheric O_2 through the Phanerozoic, revisited. *Annual Review of Earth and Planetary Sciences*, *51*(1), 253–276. https://doi.org/10.1146/annurev-earth-032320-095425

Paillard, D. (2017). The Plio-Pleistocene climatic evolution as a consequence of orbital forcing on the carbon cycle. *Climate of the Past*, *13*(9), 1259–1267. https://doi.org/10.5194/cp-13-1259-2017

Slomp, C. P., & Van Cappellen, P. (2007). The global marine phosphorus cycle: Sensitivity to oceanic circulation. *Biogeosciences*, *4*(2), 155–171. https://doi.org/10.5194/bg-4-155-2007

Tostevin, R., & Mills, B. J. W. (2020). Reconciling proxy records and models of Earth's oxygenation during the Neoproterozoic and Palaeozoic. *Interface Focus*, *10*(4), 20190137. https://doi.org/10.1098/rsfs.2019.0137

Van De Velde, S., Mills, B. J. W., Meysman, F. J. R., Lenton, T. M., & Poulton, S. W. (2018). Early palaeozoic ocean anoxia and global warming driven by the evolution of shallow burrowing. *Nature Communications*, *9*(1), 1–10. https://doi.org/10.1038/s41467-018-04973-4

West, A. J. (2012). Thickness of the chemical weathering zone and implications for erosional and climatic drivers of weathering and for carbon-cycle feedbacks. *Geology*, *40*(9), 811–814. https://doi.org/10.1130/G33041.1

Zhang, Y., Mills, B. J. W., He, T., Yang, T., & Zhu, M. (2023). Simulating the long-term carbon cycle in the Phanerozoic: Current status and future developments (in Chinese). *Chinese Science Bulletin*, *68*(12), 1580–1592. https://doi.org/10.1360/TB-2022-0813

19448007, 2025, 20, Downloaded from https://agupubs.onlinelibrary.wiley.com/doi/10.1029/2025GL118689 by NICE, National Institute for Health and Care Excellence, Wiley Online Library on [18/06/2026]. See the Terms and Conditions (https://onlinelibrary.wiley.com/terms-and-conditions) on Wiley Online Library for rules of use; OA articles are governed by the applicable Creative Commons License